Identifying Dominant Structural and Material Contributors to Enthesis Stress Redistribution Via Cotter's Method

Muhtadi Munawar Zahin,*[a] Benjamin B. Boesl [a] , and Darryl A. Dickerson [b]

[a.] Department of Mechanical and Materials Engineering, Florida International University.

[b.] Department of Chemical and Biological Engineering, University of New Mexico

*Corresponding author: mzahi002@fiu.edu

Abstract

The enthesis is a mechanically graded attachment that distributes load between soft connective tissue and bone across a severe stiffness mismatch without causing catastrophic stress concentration, making it essential for joint function. Although various structural and material features of the enthesis have been studied, their relative importance to stress redistribution remains unclear. This gap limits the design of durable replacements that reproduce enthesis mechanics. To address this issue, this study applied Cotter's method within a finite element framework to identify the features that significantly influence stress management.

Two-dimensional finite element models of the enthesis were generated with ligamentous, uncalcified fibrocartilage, calcified fibrocartilage, and subchondral bone regions. Twenty

structural and material parameters were varied across relevant ranges, and their influences were ranked using outputs measured at the ligamentous-UFC interface, tidemark, and cement line under tensile, shear, and combined loading. The results revealed that enthesis stress redistribution is governed by a limited but non-minimal subset of features. Amongst the features, the interfacial geometry at ligamentous-UFC interface was especially influential, influencing stress results both locally and distally.

These findings demonstrate that enthesis mechanics depend on coordinated interactions amongst the properties across regions. They provide a quantitative foundation for selecting design elements in enthesis repair and biomaterial replacement techniques. Overall, the study shows that the proposed technique provides a reliable and efficient framework for determining influential parameters in heterogeneous tissue mechanics.

Keywords

Enthesis, Cotter's method, Tissue characterization, Finite Element Analysis, Sensitivity Analysis, Musculoskeletal tissue mechanics, Tissue Engineering

Statement of Significance

This study introduces a novel approach to identifying key contributors to mechanical functions in the meniscal enthesis, a heterogenous tissue critical for knee joint stability. This study introduces a protocol utilizing a statistical sensitivity analysis tool on meticulously controlled Finite Element systems to quantitatively rank, from within a list of potential parameters, their relative influence on a particular output function, such as stress dispersion. By using this protocol on a simplified but physiologically relevant finite

element models, our approach provides a robust and cost-effective means of improving understanding of parameter interactions in complex heterogeneous tissues. The findings contribute to a better knowledge of meniscal enthesis function, which helps with soft tissue mechanics and biomaterial design for optimal replication.

Introduction

The enthesis is a graded fibrocartilaginous structure that anchors the soft connective tissues in the body (tendon, ligament, meniscus etc.) to the bone [1,2]. Entheses critical for joint motion and stability and serve a critical role in the function of the attached soft tissue under different types of loading [3–5], which is evident in reattachment surgeries where preserving even partial remnants of native entheses improve fixation compared to full removal [6]. Despite the large range of clinical reattachment approaches, to date, no approach has been effective in replicating the long-term durability of normal entheses, with most failing within ten years [7–10]. These failures suggest that while current methods provide anchorage, they are unable to reproduce key attributes of enthesis function [11,12]. In order to create more durable treatments for soft tissue injury, we need greater understanding of how the enthesis structure contributes to mechanical function.

To fill this knowledge gap, extensive experimental work has been performed to characterize the structural and material heterogeneity of the enthesis, with a particular focus on the areas around the tidemark, which is a visually striking representation of the transition from soft tissue to hard tissue. These studies [2,13–15] have produced important qualitative and quantitative information about enthesis features such as collagen fiber orientation, fiber disorganization, fiber stiffness, mineralization gradients, and stiffness

variations. Conventionally, structural and material properties of ligamentous region have generally been inferred from adjacent tendons or ligaments, despite the known differences in cellular, microstructure, and extracellular matrix compositions [16,17]. While these efforts provide essential insight, they do not establish the relative importance of individual structural features for mechanical function.

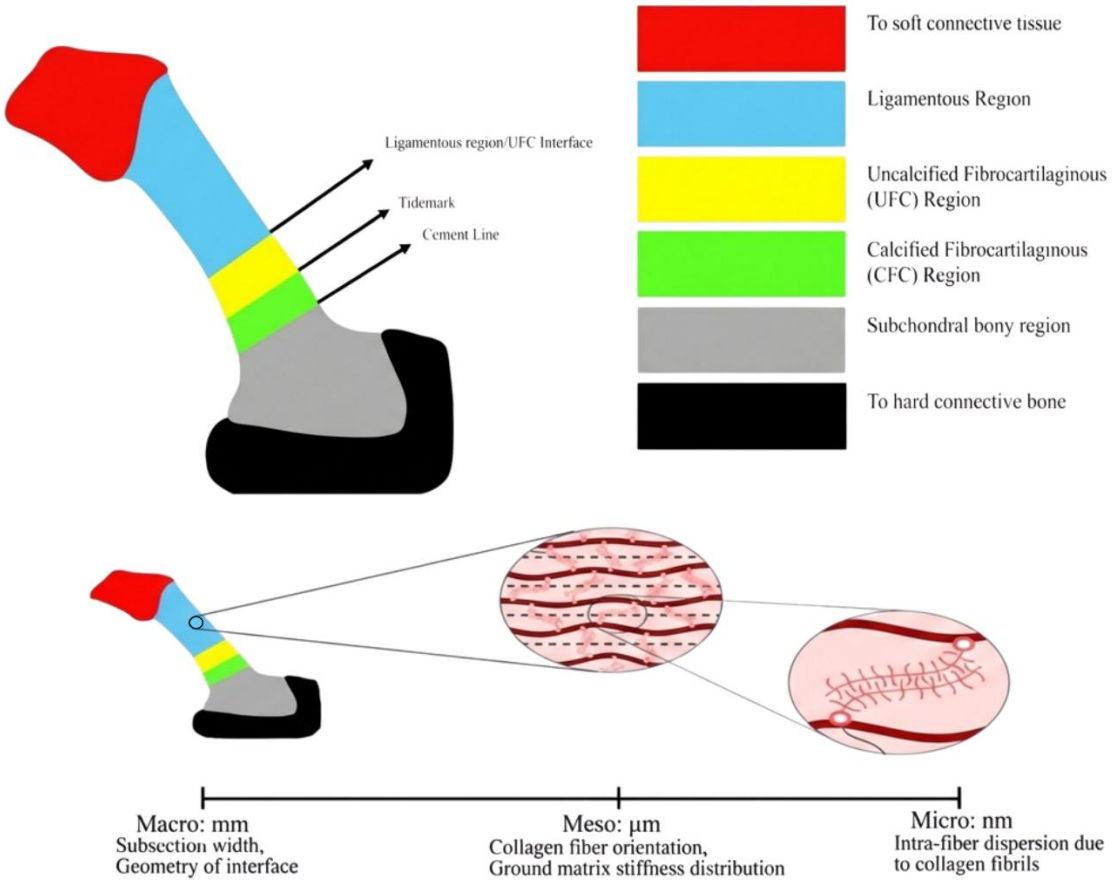

Figure 1:(Top): Schematic of a general enthesis structure with superior direction normal to view, with subregions and inter-regional interfaces distinguished with the arrows in the medial-anterior plane. (Bottom): Description of scale in terms of units and representative features in each scale.

Multiscale structural and material heterogeneity has been shown to influence enthesis mechanics. Mesoscale type I collagen fiber sliding and reorientation occur during the outset of tensile loading before load transfer through the fibrocartilaginous regions [15] which increases macroscale tensile strength. Mesoscale collagen type II collagen fiber disorganization in the UFC has been associated with increased tensile toughness, independent of graded mineralization [18–20]. At the microscale, age-related changes ECM composition further influences mechanics. Ruptured collagen type I fibers are progressively replaced by collagen type III fibers in the uncalcified regions, reflecting a shift from strength-dominance to increased toughness associated organization in the material structure [21]. Collectively, these findings indicate that multiple material and structural phenomena contribute to enthesis function at multiple length scales. However, despite extensive characterization of enthesis structural and material properties, the *relative* influence of individual features on enthesis function, particularly stress dispersion, has not yet been defined. Identifying a subset of features that are most essential to enthesis function would more clearly define structure-function relationships and provide a quantitative basis for prioritizing design criteria for biomaterial and tissue engineering strategies aimed at restoring native enthesis mechanics.

In this study, we quantify the relative influence of twenty distinct enthesis structural and material features on stress magnitude and stress concentration at enthesis sub-region interfaces under multiple loading conditions. A detailed finite element model of the enthesis was developed and parameterized across the twenty features across

physiologically relevant ranges. Using Cotter's method, the parameters describing the features were systematically varied and ranked according to their influence on stress distributions under tensile, shear, and combined loading conditions. The underlying hypothesis is that enthesis function is strongly governed by a limited subset of parameters that exert first-order control over stress redistribution.

Methods

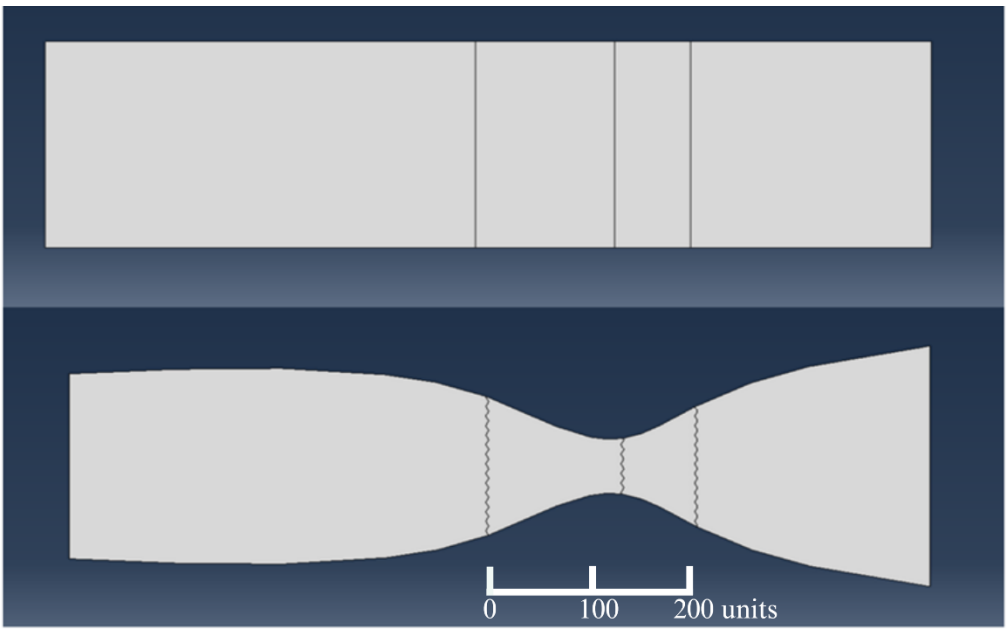

Figure 2:Comparison between two variations of the TS1 test set, to highlight macroscale geometric differences of the models used

Finite Element Model of the Meniscal Enthesis

All simulations were conducted in Abaqus/CAE 2019. The enthesis was represented as a two-dimensional, idealized, multi-region continuum composed of ligamentous, uncalcified fibrocartilage, calcified fibrocartilage, and subchondral bone regions. Regions were defined to represent experimentally reported transitions in

composition and mechanical behavior rather than reproducing a specific anatomical specimen, enabling systematic analysis across the parameter variations. Interfaces between adjacent regions were defined explicitly within the model and as part of the mesh. In some model variants, geometric perturbations were introduced at the interfaces between regions as a part of sensitivity analysis.

Models were implemented as two-dimensional shell models symmetric about the midline. This simplification was chosen because enthesis thickness is relatively constant the meniscal entheses in the superior-inferior direction, and major macroscale geometric changes are in the medial-anterior planes [27]. Thus, the 2D representation captures the primary macroscale and microscale features relevant to load transfer while reducing computational cost.

All regions were modeled using the Holzapfel-Gasser-Odgen (HGO) constitutive formulation available in Abaqus [22,26], enabling explicit control over the orientation and dispersion of fiber strands via the inclusion of terms in the anisotropic contribution in the strain energy functions. Spatial variation of material parameters within regions was implemented with temperature-dependent material properties linked to the prescribed thermal gradients. Meshes were generated using adaptive meshing and manually inspected to ensure stability. Nodes were either repositioned or removed to correct instability.

Mechanical Loading and Boundary Conditions

All models were subjected to three loading conditions: pure tension, pure shear, and combined tension-shear (termed complex loading). Rigid boundary conditions were applied to the outer edge of the ligamentous region. Loading was applied as a linearly

increasing surface traction to the undeformed outer edge of the subchondral bone region, oriented at 0º, 90º, and 45º relative to the model length for tensile, shear, and complex loading, respectively. All simulations were performed using a static, explicit step with nonlinear geometry enabled and solved using a direct equation solver with full Newton iteration for each simulation.

Computational Output Measures

Mechanical response to loading was quantified using two primary stress-based measures: average stress and stress concentration, derived from the equivalent (von Mises) stress. Stress values were taken at nodes located along internal interfaces (the LIG/UFC interface, the tidemark, and the cement line). At each interface, minimum (N_i) and maximum (H_i) nodal stresses were recorded. Average stress was defined as the mean of the nodal value stress at a given interface:

$$A_i = \frac{(H_i + N_i)}{2} \tag{1}$$

Stress concentration was defined based on the difference between min and max nodal stress values at the interface, capturing local stress amplification associated with interface geometry and material properties:

$$J_i = |H_i + N_i| \tag{2}$$

For each model and loading condition, both average stress and stress concentration were computed at each internal interface.

Sensitivity Analysis

Sensitivity analysis was used to quantify how systematic variations in structural and material features influence the stress based output measures defined above. A global screening sensitivity approach was used to rank a relatively large number of features while remaining computationally manageable. Cotter's method was selected as the screening framework for this reason.

Parameter Definition and Test Set Design

Twenty distinct structural and materials features (henceforth parameters) were assessed for their influence on the stress dispersion function of the enthesis. These parameters were selected based on prior experimental and computational literature relevant to enthesis mechanics. Parameter ranges were chosen to span physiologically relevant values and are summarized in Table 1 and Table 2.

To ensure meaningful application of the statistical analysis using Cotter's method, the parameters were organized into four testing sets. A **validation set (VS)** was used to **confirm that** the presence of fibrocartilaginous regions produced stress responses consistent with prior computational and experimental observations [5,23] [28,29]. **Testing set 1 (TS1) focused** on macroscale geometric and structural parameters (Table 1). **Testing set 2 (TS2)** assessed structural parameters while excluding macroscale geometry. The geometry of this set was taken as an internal portion of the model in TS1 that existed in both variations concerning Macroscale geometry. **Testing set 3 (TS3)** evaluated the influence of material parameters while maintaining TS2 geometry (Table 2). Interdigitation

geometry was included in TS3 to enable qualitative assessments between TS2 and TS3. Across all sets, a total of 82 enthesis model variations were generated.

Application of Cotter's Method

Cotter's method was used as the analytical tool to determine the influence of each parameter (subscript i, for total n parameters) on the stress-based output measured define above. To enable screening-based sensitivity analysis, parameters were evaluated using a binary ON/OFF formulation, where OFF and ON corresponded to the low-end and high-end values of each parameter within its prescribed range, respectively. For parameters defined by feature presence, these states corresponded to absence (OFF) and presence (ON).

For each parameter *i*, sensitivity was assessed use outputs from four reference states in the screening design: 1) all the parameters investigated have OFF value (V_0), 2) only parameter in question has ON value(V_i), 3) only parameter in question has OFF value (V_{n+i}), and 4) all parameters have ON value (V_{2n+1}). From there, three Cotter's values can be obtained [24]. Cotter's odd order effect was defined as:

$$CO_i = \frac{(V_{2n+1} - V_{n+i}) + (V_i - V_0)}{4} \tag{3}$$

representing the cumulative odd-order contributions of parameter *i*. Cotter's even order effect was defined as

$$CE_i = \frac{(V_{2n+1} - V_{n+i}) - (V_i - V_0)}{4} \tag{4}$$

And captures even-order contributions associated with co-dependent effects. Cotter's order magnitude was defined as:

$$M_i = |CO_i| + |CE_i| \tag{5}$$

Providing a measure of the overall influence of parameter *i* on the selected output measure.

To compare relative parameter influence within each test set, order magnitudes were normalized as following:

$$N_i = \frac{M_i}{\sum_{i=1}^{n} M_i} \tag{6}$$

With the exception of overall macroscale geometry which was excluded due to the outlier magnitude.

Identification of Influential Parameters

To establish the global distribution of influence across model features, normalized influence values from the Cotter sensitivity analysis were examined across all mechanical outputs. Influence was evaluated for two stress measures (average stress and stress concentration) at three interfaces (LIG–UFC, tidemark, and cement line) under three loading regimes (tensile, shear, and complex), yielding 18 output conditions. Influence values were pooled across outputs and ranked by cumulative contribution, and a Pareto-like threshold was used to identify features accounting for the majority of influence. This global assessment was used to distinguish dominant influencing features from those with

negligible contributions and to provide context for subsequent interface- and loading-specific analyses.

To provide for a more condensed outlook on the parameters, a third assessment was done by averaging the results of equation (5) for all the interfaces for a particular loading case and stress-related output. This averaged value was then normalized in accordance to equation (6) to form an averaged relative parameter influence. While this approach introduces some errors due to influence on each interface being distinct, it provides a more accessible representation of the global influence of the parameters.

Validation and Verification

Direct experimental validation is challenging for this study because the relative influence of parameters in the enthesis has not been investigated and, in many cases, cannot be performed experimentally. However, verification and limited validation were performed. The validation set was used to confirm inclusion of fibrocartilaginous regions matched prior computational studies [5,23] and experimental studies [28,29]. Verification was performed by repeating simulations for all loading cases for each model with at least 3 different mesh sizes. Average stress along the tidemark probe was used for verification. A model was considered to be verified either when there was clear convergence as mesh size was decreased.

Parameter Name	Abaqus Input	High Value	Low Value	Reference
Overall Geometry	2D shell in Sketch	Irregular Hourglass-like shape based on bovine meniscal enthesis	Equivalent rectangle to the bovine meniscal enthesis	[27]
Fiber orientation Ligamentous region	Material orientation for HGO	25º with respect to horizontal direction of enthesis	45º with respect to horizontal direction of enthesis	[14]
Fiber disorganization in ligamentous region	Kappa value of HGO material	(1/15)	(1/30)	[14,30]
Fiber orientation UFC region	Material orientation for HGO	52º with respect to horizontal direction of enthesis	48º with respect to horizontal direction of enthesis	[31]
Fiber disorganization in UFC region	Kappa value of HGO material	(1/15)	(1/18)	[30,31]
Fiber orientation CFC region	Material orientation for HGO	42º with respect to horizontal direction of enthesis	46º with respect to horizontal direction of enthesis	[31]

Parameter Name	Abaqus Input	High Value	Low Value	Reference
Fiber disorganization in CFC region	Kappa value of HGO material	(2/15)	(8/75)	[30,31]
Intra-fiber dispersion ligamentous region	k2 value of HGO material	35	5	[22]
Intra-fiber dispersion UFC region	k2 value of HGO material	35	5	[22]
Geometry of Cement line	Section separation via sketch	Sinusoidal	Straight	Modified recreation [31]
Geometry of Tidemark	Section separation via sketch	Sinusoidal	Straight	Modified recreation [31]
Presence of UFC and CFC	Inclusion of UFC and CFC region in the model	Included	Excluded	Validation assumption
Geometry of LIG/UFC interface	Section separation via sketch	Sinusoidal	Straight	Assumption

Table 1: Details and Justifications of sets VS,TS1 and TS2

Parameter Name	Abaqus Input	High Value	Low Value	Reference
Ligamentous region Ground matrix stiffness	C10 value	5MPa	10 MPa	[31]
Ligamentous region fiber stiffness	K1 value	100MPa	120MPa	[32]
UFC region Ground matrix stiffness Gradient	C10 value changed over length using temperature gradient	2-8MPa starting from LIG/UFC interface to Tidemark	2-14MPa starting from LIG/UFC interface to Tidemark	[31]
UFC region Fiber stiffness magnitude	K1 value	80MPa	60MPa	[32,33]
UFC region fiber disorganization gradient	Kappa value changed over length using temperature gradient	(1/30) to (1/15) starting from LIG/UFC interface to Tidemark	(1/30) to (1/10) starting from LIG/UFC interface to Tidemark	[15]
CFC region Ground matrix stiffness Gradient	C10 value changed over length using temperature gradient	150-600MPa starting from tidemark to cement line	150-1050MPa starting from tidemark to cement line	[31,34]
CFC region Fiber rate of crystallization	K1 value changed over length using temperature gradient	80-3900MPa starting from tidemark to cement line	80-7720MPa starting from tidemark to cement line	[31,34]
SB region stiffness magnitude	C10 and K1 value (virtual fiber assumed)	3900MPa	7720MPa	[[35] with adjustment]

Parameter Name	Abaqus Input	High Value	Low Value	Reference
CFC region Ground matrix stiffness Gradient	C10 value changed over length using temperature gradient	150-600MPa starting from tidemark to cement line	150-1050MPa starting from tidemark to cement line	[31,34]
CFC region Fiber rate of crystallization	K1 value changed over length using temperature gradient	80-3900MPa starting from tidemark to cement line	80-7720MPa starting from tidemark to cement line	[31,34]
SB region stiffness magnitude	C10 and K1 value (virtual fiber assumed)	3900MPa	7720MPa	[[35] with adjustment]

Table 2: Details and justification of parameters in Set TS3

Results

Validation and verification

The validation study (VS) demonstrated that inclusion of graded fibrocartilaginous regions has a significant effect on both average stress and stress concentration at the tidemark under loading. This finding is consistent with prior experimental studies [28,29], in which comparisons among biphasic enthesis constructs, enthesis replicants with graded regions, and native entheses, showed that the presence of graded regions produce stress concentration patterns distinct from those of a pure biphasic scaffold. All loading cases were verified using a minimum of three mesh densities per loading scenario. Mesh convergence was assessed at tidemark region for each loading case to ensure consistency across simulations. Detailed validation and verification results are provided in the supplemental information.

Global examination of influential features

The aim of this initial analysis was to identify which individual enthesis features contribute meaningfully when influence is aggregated across all functional outputs, including stress magnitude and stress concentration, all loading regimes, and all interfacial locations. This global examination was not intended to localize effects or infer mechanisms, but rather to establish whether influence is broadly distributed across parameters or organized hierarchically prior to more focused analyses.

First, in simulation sets examining macroscale geometry, this feature exhibited dominant global influence, with a mean normalized Cotter's index excess of 0.95 in most

test cases. Across simulation spaces, global influence was not evenly distributed. In the structural organization space (TS2), influence was concentrated in a subset of parameters associated with interfacial geometry and fiber orientation. Interdigitation at the UFC–ligamentous interface exhibited the largest mean normalized influence (0.240), followed by interdigitation at the cement line (0.177) and tidemark (0.165). Among fibrous parameters, ligamentous region fiber orientation (0.138) and UFC fiber orientation (0.106) were the most influential, whereas fiber dispersion and intrafiber dispersion parameters contributed comparatively little. In total, seven of eleven structural parameters accounted for more than 90% of cumulative global influence, indicating a clear hierarchy in structural contributions within these parameters.

A similar pattern was found in the material property gradient space (TS3), although the dominant features differed. Ligamentous region ground matrix stiffness magnitude exhibited the largest global influence (0.312), with additional contributions from ground matrix stiffness gradients in the calcified fibrocartilage (0.136) and UFC regions (0.101). Interdigitation at the UFC–ligamentous interface (0.103) and tidemark (0.133) also contributed substantially, while fiber stiffness, crystallization gradients, and fiber disorganization gradients had relatively minor influence. Here, six of eleven parameters accounted for over 90% of cumulative global influence.

Together, these results show that enthesis stress outcomes are governed by a limited but non-minimal subset of features, characterized by a small number of dominant contributors and some features that demonstrate weak effects. This hierarchical structure

motivates subsequent examination of how these dominant features influence stress management at specific interfaces and under distinct loading regimes.

Interface specific patterns of feature influence

To examine how stress outcomes vary locally, influence was next aggregated by interface, pooling all loading regimes and stress measures. This interface-specific perspective reveals systematic differences in which features contribute most strongly to stress magnitude and stress concentration, while also highlighting a small number of contributors that remain influential across interfaces.

At the tidemark, influence was concentrated in parameters associated with interfacial geometry and material transitions (FIG 3,4). In the structural organization space (TS2), tidemark interdigitation accounted for the largest share of cumulative influence, accompanied by consistent contributions from ligamentous and UFC fiber orientation, which remained among the most influential fibrous parameters. Fiber dispersion and intrafiber dispersion parameters contributed minimally. A similar hierarchy was observed in the material property gradient space (TS3), where tidemark interdigitation, ligamentous ground matrix stiffness magnitude, and stiffness gradients within the calcified fibrocartilage and UFC regions together accounted for the majority of influence.

At the LIG-UFC interface, influence was more tightly localized to the immediately adjacent regions (FIG 3,4). Structurally, LIG-UFC interdigitation exhibited the greatest influence, with ligamentous and UFC fiber orientation again contributing prominently, while parameters associated with the calcified fibrocartilage were negligible. In the

material space, ligamentous ground matrix stiffness magnitude dominated influence, with secondary contributions from the UFC stiffness gradient and interdigitation at the interface.

At the cement line, dominant contributors shifted toward features associated with the calcified fibrocartilage and subchondral bone (FIG 3,4). Structurally, cement line interdigitation accounted for the largest share of influence; however, ligamentous and UFC fiber orientation continued to contribute non-negligibly, whereas dispersion-related parameters remained minor. In the material space, stiffness magnitude of the subchondral bone and stiffness gradients within the calcified fibrocartilage were the most influential parameters for this set.

Collectively, these results show that dominant features differ systematically by interface, with stress regulation governed by interfacial geometry at transition zones and by regional material properties proximal to the interface. Regardless of interface location, fiber orientation exerts significant influence in stress management.

Stress management across loading regimes

To determine whether dominant stress management mechanisms persist across loading directions or are activated conditionally, influence was evaluated separately under combined (complex), tensile, and shear loading, and parameters contributing to the primary influencing features were identified for each loading regime. Under complex loading, functional outputs of the enthesis were most influenced by interfacial geometry, ligamentous and UFC fiber orientation, and ligamentous ground matrix stiffness magnitude. In the structural organization space, LIG-UFC, tidemark, and cement line interdigitation together accounted for a substantial fraction of cumulative influence,

accompanied by ligamentous and UFC fiber orientation. In the material property gradient space, ligamentous ground matrix stiffness magnitude, stiffness gradients in the UFC and calcified fibrocartilage, and subchondral bone stiffness magnitude were retained within the dominant feature set. Under tensile loading, this core set was largely preserved; however, additional parameters associated with the calcified fibrocartilage, including fiber orientation, fiber dispersion, and stiffness gradients, entered the dominant feature set. These parameters were not retained under combined loading, indicating loading-activated sensitivity to fibrocartilaginous organization under axial loading. Under shear loading, influence shifted toward parameters associated with ligamentous fiber dispersion and disorganization, which were retained within the dominant feature set under shear but not under combined or tensile loading. Interfacial geometry and ligamentous ground matrix stiffness magnitude remained influential, but the relative contribution of fiber orientation decreased compared to dispersion-related parameters.

Across all loading regimes, a consistent set of dominant influencing features were identified, including interfacial geometry at the LIG–UFC, tidemark, and cement line interfaces; mean fiber orientation in the LIG and UFC regions; and LIG ground matrix stiffness magnitude.

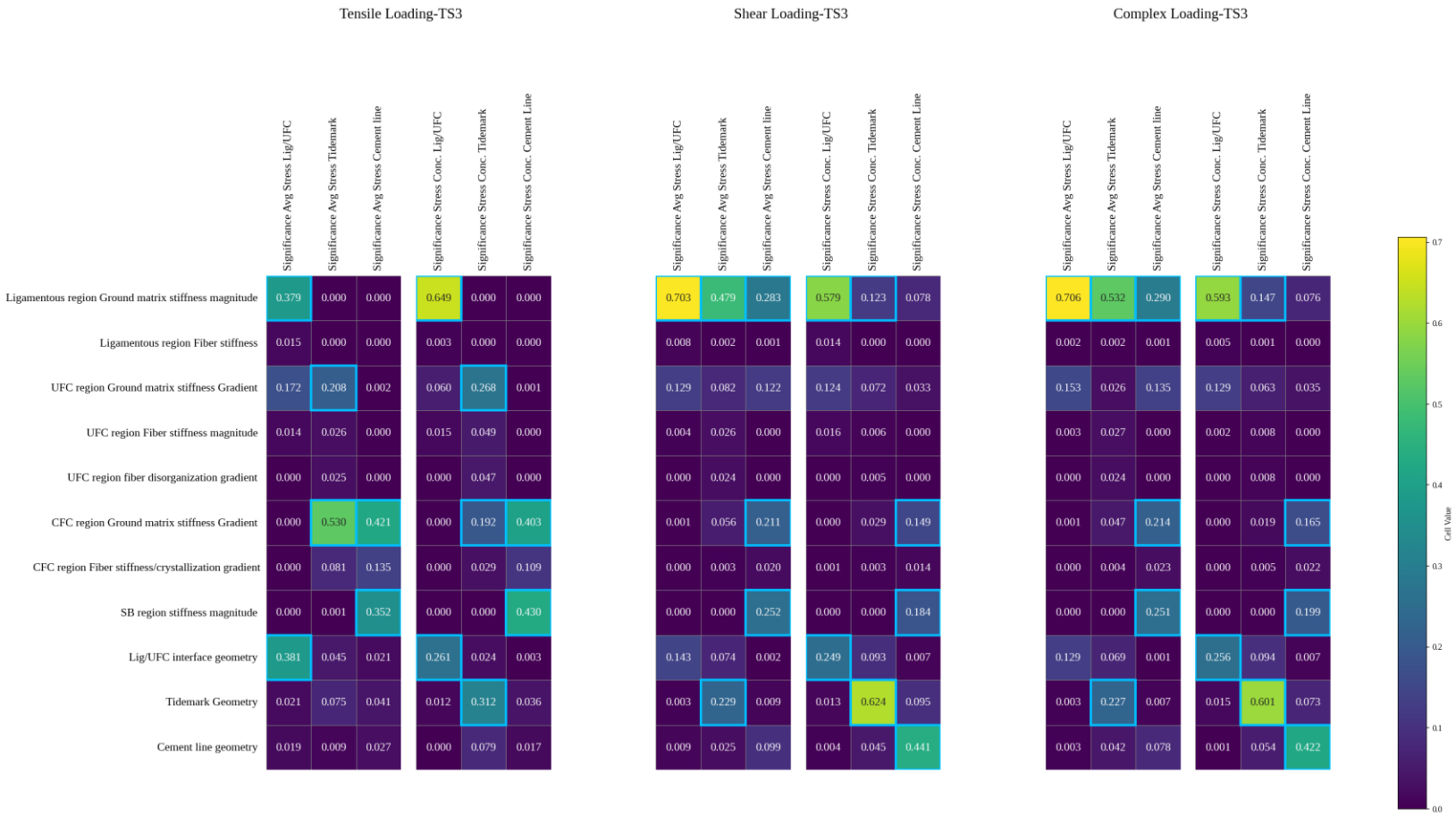

Figure 3: Heatmap for relative influence of parameters in TS3, with parameters considered to be significant highlighted in blue.

Figure 4: Heatmap for relative influence of parameters in TS2, with parameters considered to be significant highlighted in blue

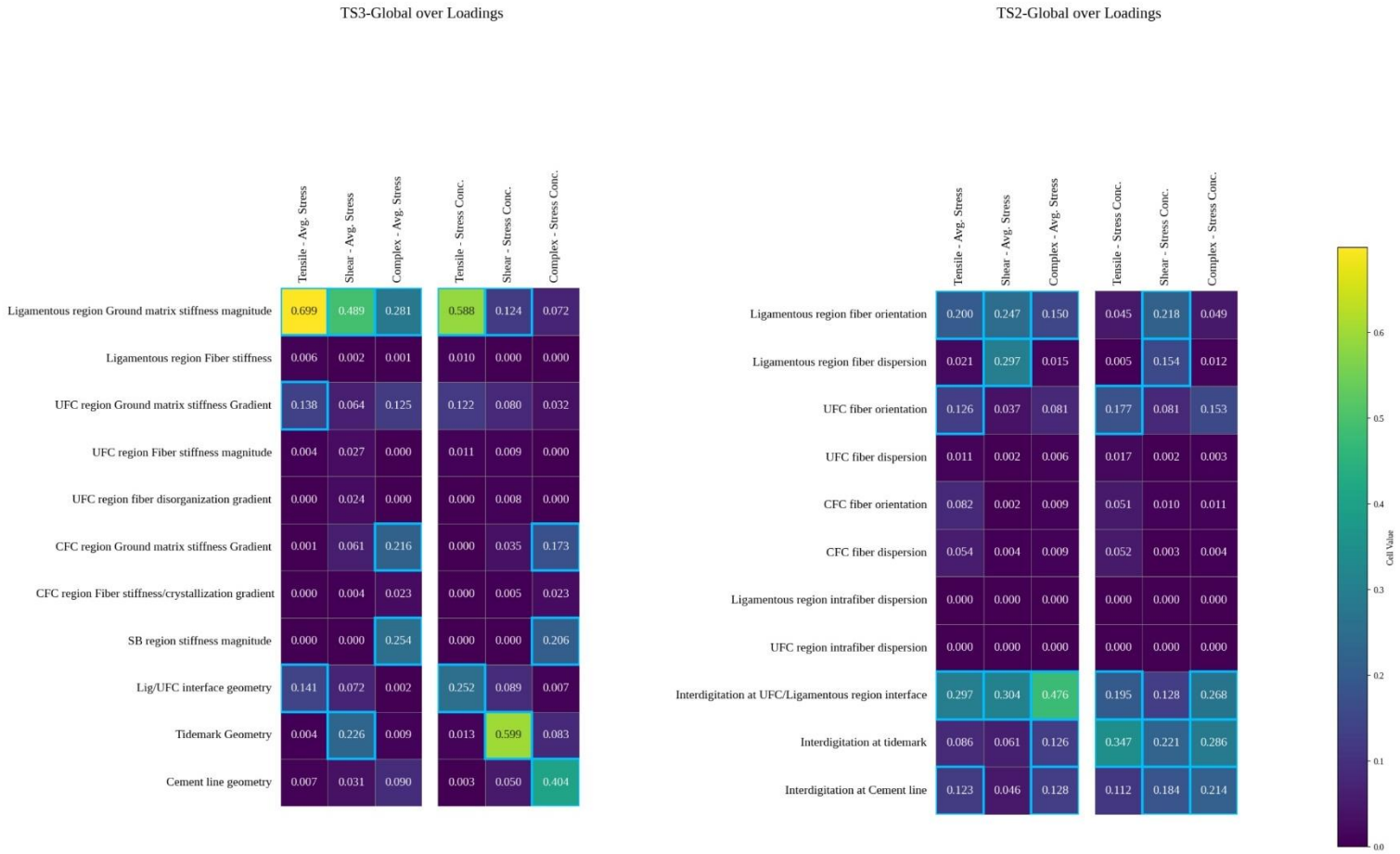

Figure 5: Heatmap of parameters from TS2 (right) and TS3 (left), with relative influences averaged and normalized of all 3 interfaces for each loading case

Parameter Name	Significant in Tensile Loading	Significant in Shear loading	Significant in Combined loading
Overall Geometry			
Fiber orientation Ligamentous region			
Fiber disorganization in ligamentous region			
Fiber orientation UFC region			
Fiber disorganization in UFC region			
Fiber orientation CFC region			
Fiber disorganization in CFC region			
Intra-fiber dispersion ligamentous region			
Intra-fiber dispersion UFC region			
Geometry of Cement line			
Geometry of Tidemark			
Geometry of LIG/UFC interface			
Ligamentous region Ground matrix stiffness			

Ligamentous region fiber stiffness			
UFC region Ground matrix stiffness Gradient			
UFC region Fiber stiffness magnitude			
UFC region fiber disorganization gradient			
CFC region Ground matrix stiffness Gradient			
CFC region Fiber rate of crystallization			
SB region stiffness magnitude			

Table 3: Binary chart summarizing parameters influential (Colored green) in each of the loading cases

Discussion

The objective of this study was to identify which structural and material features of the enthesis had the most significant influence on the stress dispersion function under physiologically relevant loading. Using finite element modeling combined with Cotter's method, we quantified

the relative influence of twenty parameters across several enthesis inter-regional interfaces and loading conditions. The findings showed that not all aspects of the enthesis contribute equally to its stress management function.

Heterogenous properties of enthesis and impact on stress management

The enthesis is a heterogenous structure, with numerous aspects that determine its functions. One of the primary goals of this study was to evaluate the relative influence of these parameters on the ability of the enthesis to distribute stress. This understanding is essential not only for clarifying the mechanical basis of stress dispersion, but also for guiding the design of replacement systems with comparable functional performance. A fundamental finding from this study is that enthesis function is connected to a smaller number of structural and material features that act as first order regulators of load transfer.

Among all parameters considered, macroscale geometry had the most significant influence on stress management. This study provides the first quantitative comparison demonstrating that geometry plays a critical role in stress dispersion. Its importance has been noted in clinical observations [1,28,36–38], but it has not yet been purposefully incorporated into design strategies. Based on the assumptions guiding Cotter's method, modifying the macroscale geometry changes the relative size of the enthesis subregions and consequently affects the contribution of the remaining parameters in the set. To gain a more accurate understanding of these influences, the remaining structural parameter sets were examined in a second set of analyses where macroscale geometry was kept constant, enabling a clearer assessment of their relative influence.

At the smaller structural scale, gradients in fiber orientation spanning the ligamentous area, UFC, and CFC had a significant impact on stress management [2,15]. The simulations showed that

disrupting these gradients impairs the overall stress distribution capability of the enthesis [39,40]. All transitions between the subregions were found to be significantly influential as well. Between the three interfaces, the tidemark has received the most attention [1,2,15,28,41], followed by the cement line [5]. However, the interface between the ligamentous region and UFC has received far less attention. This could be because, unlike the tidemark and cement line, it lacks a well-defined visual or compositional border. The results of the present study provide quantitative rationale for renewed attention to this interface. Notably, variations in ligament–UFC interfacial geometry influenced stress outcomes not only locally, but also at the tidemark and cement line. In contrast. changes to the other two interface geometries primarily affected stress outcomes at their respective locations. This nonlocal sensitivity suggests that the ligament–UFC interface plays a disproportionate role in stress distribution across the enthesis, despite its relatively subtle morphological appearance.

From the compositional based parameter test sets, the stiffnesses of the ground matrices in all subregions had a significant influence on stress dispersion. The gradient of the material stiffness is supported by the prior mechanical testing, which has led to prototyping efforts which focused on this aspect [42–50]. Of particular interest is the finding that it is only the stiffnesses of the ground matrices that were significant in each subregion: the stiffnesses of the fibers in each of the subregions were not found to be significantly influential, when compared to fiber orientations or ground matrix stiffnesses. This finding suggests that stress dispersion is handled by ground matrices and fibers under different mechanisms.

While this study identified the key parameters influencing stress dispersion, these factors alone do not fully explain the mechanical response of the enthesis. The overall stress management capability is derived from the interaction of several aspects rather than from any single parameter. In this

respect, effective stress dispersion mainly depends on the coordination of the identified structural and material properties.

Hierarchical organization of enthesis stress management – context dependent stress management strategies

The enthesis stress management function is governed by a subset of the present structural and compositional aspects. A consistent trend was observed in which significant parameters were continuous across the enthesis. This observation suggests that stress dispersion is influenced more inter-regional interactions rather than isolated material or structural features. Particularly, gradients in mean fiber orientation within the ligamentous and fibrocartilaginous regions, together with gradients in ground matrix stiffness had comparable influences on stress distribution, not one of the parameters overpowering the others in terms of influence. This finding aligns with previous studies showing that all four enthesis subregions contribute collectively to mechanical performance [28,29]. The results also propose a functional hypothesis of collagen fibrous tissues. Under this hypothesis, collagen fibers serve more as a stress vector than a stress resistor when implanted in a softer ECM environment. This is complemented by their stiffening during their mineralization in the harder subregions, where they then act as stress resistors. Future research on this topic could include modified HGO models. Such models can include a fiber activation term in the isotropic stiffness term, which activates the anisotropic stiffness terms only when a certain threshold value is exceeded. The results simulation of the modified model can then be compared with previous simulation results and experimental outcomes. This will result in a better knowledge of how collagenous tissue functions in general.

The interface-specific analyses show that enthesis stress regulation is spatially localized and context-dependent. Different interfaces use distinct combinations of geometric, structural, and material features to manage stress, reflecting the varying mechanical environments experienced across the enthesis. At mineralized transitions, material stiffness gradients play a more prominent role, whereas at soft tissue interfaces, tissue compliance and fiber alignment are dominant. This observation may explain why attempts to replicate enthesis function using a single design rationale, such as mineral gradients alone, have had limited success in restoring enthesis function. Therefore, a multi-faceted approach of replicating key stress dispersion pathways should be prioritized: the findings from the current work suggest the following categorization in Figure 8.

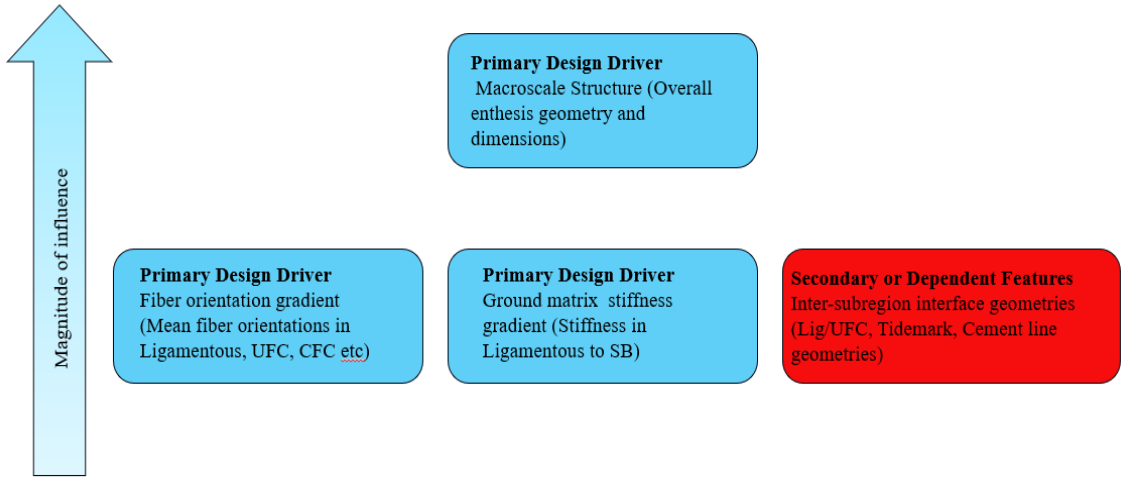

Figure 6: Visualization of influential parameter groups. From a design perspective, 2c loses priority as it can be dependent on 2a and 2b

Another key contribution of this work is the differentiation between robust stress management features (across all loading regimes) and loading activated mechanisms. Some aspects have a consistent influence regardless of loading conditions, indicating that they form a stable mechanical backbone of the enthesis. Other aspects only become influential under specific loading conditions, implying that the enthesis engages additional mechanisms in response to the particular loading conditions. This organization provides a useful framework for understanding how the enthesis

accommodates complex, multiaxial loading in vivo. Rather than relying on different mechanisms for different loads, the enthesis appears to integrate a constant foundation mechanism with context-sensitive mechanisms that modulate stress dispersion under special circumstances.

Implications for Enthesis Characterization, Repair, and Biomaterial Design

From an enthesis repair and replacement perspective, these results clarify which design features are critical for restoring mechanical function. Most importantly, effective constructs must reproduce the macroscale geometry and dimensions of the native attachment, since these aspects establish the global mechanical context. Within this framework, stress management is governed primarily by gradients in mean fiber orientation within the ligamentous and fibrocartilaginous regions and by ground matrix stiffness gradients, rather than by fiber stiffness itself. Therefore, the first two gradients gain preference in replication consideration over the last aspect.

The limited influence of fiber disorganization gradients suggests that replicating it may not be necessary for mechanical performance, but this effect may be underestimated due to modelling simplifications. Overall, the results suggest that fiber orientation should receive greater priority than fiber disorganization or individual fiber stiffness when designing mechanically functional replacements. Another crucial consideration is the shape of the ligamentous-UFC interface. Its discovered influence encourages future exploration of this interface and emphasizes the importance of high-resolution control over heterogeneous material properties in order to duplicate interfacial geometry.

More broadly, the findings indicate that the enthesis' features act in a continuous manner across subregions. A fundamental implication is that the replication of heterogeneous structures may require a shift away from evaluating influential parameters in isolation. Instead of focusing only

on individual influential parameters, future design approaches should identify which properties serve as the primary routes of stress transfer between the sub-regions, thus allowing the full heterogeneous structure to operate as an integrated system.

In practice, the findings suggest that material strategies incorporating material stiffness gradients, such as those imitating mineralization gradient [51] continue but should not be seen as a standalone solution. Strategies emphasizing orientational guidance and matrix-level stiffness transitions are likely to be more effective than approaches focused solely on compositional mimicry. A prospective replicant can use fiber composite hydrogels [52], in which the fiber strands are mixed in the hydrogel mixture and their general orientation controlled before the hydrogel mixture is set.

Methodological considerations of Cotter's method

A primary motivator for the effort to understand and duplicate the diverse entheses of the human body is their ability to disperse produced stress from a location with a significant discrepancy in material stiffness [2,15]. To date, work has been focused on characterizing a specific parameter, incorporating the characterized in a material model or replicating the parameter in an artificial replacement, and examining whether stress dispersion and increased toughness are achieved. This study demonstrates the benefits of using screening-based sensitivity analysis to help disentangle complex structure–function relationships in biological tissues.

Cotter's method provides a computationally efficient means of identifying dominant contributors without requiring exhaustive parameter sweeps [24]. The method is useful for both initial parameter screening and for guiding more focused investigations into how significant parameters act independently or in combination. Cotter's method was chosen for its systemic reproducibility, ability to further distinguish the nature of influence, robustness to variable changes, and a relatively

small number of required test cases. Alternative screening approaches considered included Plackett-Burman [53], Taguchi [54], Sobol's [55] and Morris factorial [56] methods; however, Cotter's method offered the most efficient and consistent framework for comparative studies in which interactions among enthesis features are a central focus. While experimental implementation of such methods remains challenging [57,58], finite element modeling offers a controlled environment in which relative influence can be assessed reproducibly for more accurate understanding [59–61].

The accuracy of parameter identification is highly dependent on the model's complexity and the composition of the testing sets. Cotter's method assumes that varying one input parameter or system condition does not change how the other evaluated parameters influence the output. Therefore, when strong interactions exist among parameters within the testing sets, the method may be less effective for identifying their relative importance. To accommodate for this, the structural and compositional parameters were evaluated in separate sets, ensuring that compositional aspects within a subregion did not influence structural aspects and vice versa.

For this work, several modeling simplifications were necessary, including the use of two-dimensional geometry and hyperelastic material models. Such choices limit direct quantitative comparison with experimental stress magnitudes but do not generally undermine the hierarchy of influence identified here. One probable exception to this is the fiber disorganization gradient: the results suggest that this parameter set is not sufficiently significant to enthesis stress dispersion properties. This contradicts expectations set from previous investigations [2,15,27,39,62]. One possible explanation is that the influence of fiber disorganization was reduced in the current study because it was compared relative to mean fiber orientation within the same testing set. A second possibility is that fiber disorganization has additional effects under poroelastic conditions that

hyperelastic modeling alone cannot account for. For example, increased disorganization within the fibrocartilaginous region may create greater matrix openings, leading to higher fluid-matrix interactions under mechanical loading in UFC compared to ligamentous region. Future studies should incorporate three-dimensional architecture and poroviscoelastic behavior [61,63–71] to reexamine these findings. These studies will also help to clarify the structure-function relationships of the enthesis and other heterogeneous tissues in general.

From a broader perspective, Cotter's sensitivity analysis method proved to be a reliable tool for finding influential factors and directing more extensive research of the independent and co-dependent impacts of relevant variables. In this investigation, a simplified model was intentionally used to allow key properties to be identified from a large pool of candidate parameters. As a result, identification accuracy is primarily limited by the complexity of the model and the selection of parameters within each testing set. Despite these constraints, the study successfully identified the key mechanical parameters and ranked their relative influence on stress dispersion. These findings provided insights into several mechanisms associated with the structure-function behavior of the enthesis as well as implications for replacement design. While the uncertainty surrounding fiber disorganization may be due to the simplifying assumptions used in the model, the overall hierarchy of stress-dispersion properties remains meaningful. Therefore, this work provides a solid foundation for future investigations into the independent and co-dependent influences that govern the enthesis structure-function relationship.

Conclusion

In this work, sensitivity analysis was performed across multiple finite element models to identify parameters that significantly influence average stress and stress concentration at

subregional interfaces of the meniscal enthesis. The findings reaffirm the significance of some previously examined traits, while also emphasizing features that have gotten relatively little attention. In particular, the geometry of the ligamentous–UFC interface was found to influence stress outcomes not only locally, but also at distal interfaces, emphasizing the necessity for further concentrated research into this transition region. More broadly, the findings indicate that effective stress dispersion in the meniscal enthesis depends on the combined contribution of structural organization, through collagen fiber orientation and disorganization, and compositional properties, through regional ground matrix stiffness. These findings emphasize the importance of considering these aspects simultaneously in future replacement designs.

This study also demonstrates the utility of combining Cotter's method with finite element analysis as a framework for interrogating complex biological systems. The approach provides a reliable and computationally efficient means of identifying influential parameters in multivariable systems where direct experimental exploration would be impractical due to temporal and fiscal constraints. While the method relies on assumptions of parameter independence and constancy of non-variable inputs, it nevertheless offers a powerful, quantitative basis for prioritizing tissue properties that are most crucial for recreating the intended mechanical performance, especially in heterogenous structures.

Author contributions

Muhtadi Munawar Zahin: Investigation, Methodology, Formal Analysis, Data Curation, Visualization, Validation, Writing-original draft, Writing-review & editing

Benjamin B. Boesl: Supervision, Writing-review & editing

Darryl A. Dickerson: Conceptualization, Methodology, Resources, Supervision, Writing-review & editing, Project administration, Funding acquisition

Data Availability

All of the modelling files, raw output charts, Cotter's value calculation and supplementary files are publicly available at https://osf.io/83cpm .

Conflicts of interest

The authors state that "There are no conflicts to declare".

Bibliography

[1] S. Thomopoulos, V. Birman, G.M. Genin, Structural interfaces and attachments in biology, Springer Science & Business Media, 2012.

[2] A.C. Abraham, T.L. Haut Donahue, From meniscus to bone: A quantitative evaluation of structure and function of the human meniscal attachments, Acta Biomater. 9 (2013) 6322–6329. https://doi.org/10.1016/j.actbio.2013.01.031.

[3] A.C. Abraham, D.F. Villegas, K.R. Kaufman, T.L. Haut Donahue, Internal pressure of human meniscal root attachments during loading, J. Orthop. Res. 31 (2013) 1507–1513. https://doi.org/10.1002/jor.22408.

[4] L. Zhao, A. Thambyah, N.D. Broom, A multi-scale structural study of the porcine anterior cruciate ligament tibial enthesis, J. Anat. 224 (2014) 624–633. https://doi.org/10.1111/joa.12174.

[5] V. Birman, G.M. Genin, S. Thomopoulos, Multiscale Enthesis Mechanics, in: O.T. Thomsen, C. Berggreen, B.F. Sorensen (Eds.), 20th Int. Conf. Compos. Mater., Aalborg Univ Press, Aalborg, 2015. https://www.webofscience.com/wos/woscc/full-record/WOS:000614628003092 (accessed January 16, 2023).

[6] W. Su, X. Li, S. Zhao, P. Shen, S. Dong, J. Jiang, J. Zhao, Native Enthesis Preservation Versus Removal in Rotator Cuff Repair in a Rabbit Model, Arthrosc. J. Arthrosc. Relat. Surg. 34 (2018) 2054–2062. https://doi.org/10.1016/j.arthro.2018.03.005.

[7] P.C.M. Verdonk, K.L. Verstraete, K.F. Almqvist, K. De Cuyper, E.M. Veys, G. Verbruggen, R. Verdonk, Meniscal allograft transplantation: Long-term clinical results with radiological

and magnetic resonance imaging correlations, Knee Surg. Sports Traumatol. Arthrosc. 14 (2006) 694–706. https://doi.org/10.1007/s00167-005-0033-2.
[8] P. Henry, D. Wasserstein, S. Park, T. Dwyer, J. Chahal, G. Slobogean, E. Schemitsch, Arthroscopic Repair for Chronic Massive Rotator Cuff Tears: A Systematic Review, Arthrosc. J. Arthrosc. Relat. Surg. 31 (2015) 2472–2480. https://doi.org/10.1016/j.arthro.2015.06.038.
[9] P. Ajrawat, T. Dwyer, M. Almasri, C. Veillette, A. Romeo, T. Leroux, J. Theodoropoulos, A. Nauth, P. Henry, J. Chahal, Bone marrow stimulation decreases retear rates after primary arthroscopic rotator cuff repair: a systematic review and meta-analysis, J. Shoulder Elbow Surg. 28 (2019) 782–791. https://doi.org/10.1016/j.jse.2018.11.049.
[10] U.G. Longo, A. Carnevale, I. Piergentili, A. Berton, V. Candela, E. Schena, V. Denaro, Retear rates after rotator cuff surgery: a systematic review and meta-analysis, BMC Musculoskelet. Disord. 22 (2021) 749. https://doi.org/10.1186/s12891-021-04634-6.
[11] A. Masferrer-Pino, I. Saenz-Navarro, G. Rojas, S. Perelli, J. Erquicia, P.E. Gelber, J.C. Monllau, The Menisco-Tibio-Popliteus-Fibular Complex: Anatomic Description of the Structures That Could Avoid Lateral Meniscal Extrusion, Arthrosc. J. Arthrosc. Relat. Surg. 36 (2020) 1917–1925. https://doi.org/10.1016/j.arthro.2020.03.010.
[12] M.D. Crema, F.W. Roemer, D.T. Felson, M. Englund, K. Wang, M. Jarraya, M.C. Nevitt, M.D. Marra, J.C. Torner, C.E. Lewis, A. Guermazi, Factors Associated with Meniscal Extrusion in Knees with or at Risk for Osteoarthritis: The Multicenter Osteoarthritis Study, Radiology 264 (2012) 494–503. https://doi.org/10.1148/radiol.12110986.
[13] J. Gao, Immunolocalization of types I, II, and X collagen in the tibial insertion sites of the medial meniscus, Knee Surg. Sports Traumatol. Arthrosc. 8 (2000) 61–65. https://doi.org/10.1007/s001670050013.
[14] J. Du, A.J.-T. Chiang, C.B. Chung, S. Statum, R. Znamirowski, A. Takahashi, G.M. Bydder, Orientational analysis of the Achilles tendon and enthesis using an ultrashort echo time spectroscopic imaging sequence, Magn. Reson. Imaging 28 (2010) 178–184. https://doi.org/10.1016/j.mri.2009.06.002.
[15] A.J. Boys, J.A.M.R. Kunitake, C.R. Henak, I. Cohen, L.A. Estroff, L.J. Bonassar, Understanding the Stiff-to-Compliant Transition of the Meniscal Attachments by Spatial Correlation of Composition, Structure, and Mechanics, ACS Appl. Mater. Interfaces 11 (2019) 26559–26570. https://doi.org/10.1021/acsami.9b03595.
[16] J.L. Puetzer, T. Ma, I. Sallent, A. Gelmi, M.M. Stevens, Driving Hierarchical Collagen Fiber Formation for Functional Tendon, Ligament, and Meniscus Replacement, Biomaterials 269 (2021) 120527. https://doi.org/10.1016/j.biomaterials.2020.120527.
[17] M.E. Brown, J.L. Puetzer, Driving native-like zonal enthesis formation in engineered ligaments using mechanical boundary conditions and β-tricalcium phosphate, Acta Biomater. 140 (2022) 700–716. https://doi.org/10.1016/j.actbio.2021.12.020.
[18] N. Liu, J. Jiang, T. Liu, H. Chen, N. Jiang, Compositional, Structural, and Biomechanical Properties of Three Different Soft Tissue–Hard Tissue Insertions: A Comparative Review, ACS Biomater. Sci. Eng. 10 (2024) 2659–2679. https://doi.org/10.1021/acsbiomaterials.3c01796.
[19] Y. Liu, S. Thomopoulos, C. Chen, V. Birman, M.J. Buehler, G.M. Genin, Modelling the mechanics of partially mineralized collagen fibrils, fibres and tissue, J. R. Soc. Interface (2014). https://doi.org/10.1098/rsif.2013.0835.

[20] A.C. Deymier, Y. An, J.J. Boyle, A.G. Schwartz, V. Birman, G.M. Genin, S. Thomopoulos, A.H. Barber, Micro-mechanical properties of the tendon-to-bone attachment, Acta Biomater. 56 (2017) 25–35. https://doi.org/10.1016/j.actbio.2017.01.037.
[21] D.P. Cury, F.J. Dias, M.A. Miglino, I. Watanabe, Structural and Ultrastructural Characteristics of Bone-Tendon Junction of the Calcaneal Tendon of Adult and Elderly Wistar Rats, PLOS ONE 11 (2016) e0153568. https://doi.org/10.1371/journal.pone.0153568.
[22] U. Huh, C.-W. Lee, J.-H. You, C.-H. Song, C.-S. Lee, D.-M. Ryu, Determination of the Material Parameters in the Holzapfel-Gasser-Ogden Constitutive Model for Simulation of Age-Dependent Material Nonlinear Behavior for Aortic Wall Tissue under Uniaxial Tension, Appl. Sci. 9 (2019) 2851. https://doi.org/10.3390/app9142851.
[23] Y. Liu, V. Birman, C. Chen, S. Thomopoulos, G.M. Genin, Mechanisms of Bimaterial Attachment at the Interface of Tendon to Bone, J. Eng. Mater. Technol. 133 (2011) 011006. https://doi.org/10.1115/1.4002641.
[24] S.C. COTTER, A screening design for factorial experiments with interactions, Biometrika 66 (1979) 317–320. https://doi.org/10.1093/biomet/66.2.317.
[25] G.A. Holzapfel, T.C. Gasser, A viscoelastic model for fiber-reinforced composites at finite strains: Continuum basis, computational aspects and applications, Comput. Methods Appl. Mech. Eng. 190 (2001) 4379–4403. https://doi.org/10.1016/S0045-7825(00)00323-6.
[26] T.C. Gasser, R.W. Ogden, G.A. Holzapfel, Hyperelastic modelling of arterial layers with distributed collagen fibre orientations, J. R. Soc. Interface 3 (2006) 15–35. https://doi.org/10.1098/rsif.2005.0073.
[27] D.F. Villegas, T.A. Hansen, D.F. Liu, T.L. Haut Donahue, A quantitative study of the microstructure and biochemistry of the medial meniscal horn attachments, Ann. Biomed. Eng. 36 (2008) 123–131. https://doi.org/10.1007/s10439-007-9403-x.
[28] A.J. Boys, M.C. McCorry, S. Rodeo, L.J. Bonassar, L.A. Estroff, Next generation tissue engineering of orthopedic soft tissue-to-bone interfaces, MRS Commun. 7 (2017) 289–308. https://doi.org/10.1557/mrc.2017.91.
[29] M.C. McCorry, M.M. Mansfield, X. Sha, D.J. Coppola, J.W. Lee, L.J. Bonassar, A model system for developing a tissue engineered meniscal enthesis, Acta Biomater. 56 (2017) 110–117. https://doi.org/10.1016/j.actbio.2016.10.040.
[30] T.C. Gasser, R.W. Ogden, G.A. Holzapfel, Hyperelastic modelling of arterial layers with distributed collagen fibre orientations, J. R. Soc. Interface 3 (2006) 15–35. https://doi.org/10.1098/rsif.2005.0073.
[31] A.C. Abraham, T.L. Haut Donahue, From meniscus to bone: A quantitative evaluation of structure and function of the human meniscal attachments, Acta Biomater. 9 (2013) 6322–6329. https://doi.org/10.1016/j.actbio.2013.01.031.
[32] N. Chandrashekar, H. Mansouri, J. Slauterbeck, J. Hashemi, Sex-based differences in the tensile properties of the human anterior cruciate ligament, J. Biomech. 39 (2006) 2943–2950. https://doi.org/10.1016/j.jbiomech.2005.10.031.
[33] N. Vázquez-Portalatín, C.E. Kilmer, A. Panitch, J.C. Liu, Characterization of Collagen Type I and II Blended Hydrogels for Articular Cartilage Tissue Engineering, Biomacromolecules 17 (2016) 3145–3152. https://doi.org/10.1021/acs.biomac.6b00684.
[34] D. Qu, S.D. Subramony, A.L. Boskey, N. Pleshko, S.B. Doty, H.H. Lu, Compositional mapping of the mature anterior cruciate ligament-to-bone insertion, J. Orthop. Res. 35 (2017) 2513–2523. https://doi.org/10.1002/jor.23539.

[35] P.L. Mente, J.L. Lewis, Elastic modulus of calcified cartilage is an order of magnitude less than that of subchondral bone, J. Orthop. Res. 12 (1994) 637–647. https://doi.org/10.1002/jor.1100120506.
[36] A.J. Krych, M.D. LaPrade, M. Hevesi, N.G. Rhodes, A.C. Johnson, C.L. Camp, M.J. Stuart, Investigating the Chronology of Meniscus Root Tears: Do Medial Meniscus Posterior Root Tears Cause Extrusion or the Other Way Around?, Orthop. J. Sports Med. 8 (2020) 1–7. https://doi.org/10.1177/2325967120961368.
[37] S.R. Sundararajan, R. Ramakanth, A.S. Sethuraman, M. Kannan, S. Rajasekaran, Correlation of factors affecting correction of meniscal extrusion and outcome after medial meniscus root repair, Arch. Orthop. Trauma Surg. (2021). https://doi.org/10.1007/s00402-021-03870-8.
[38] P.L. Wilson, C.W. Wyatt, J. Romero, M.J. Sabatino, H.B. Ellis, Incidence, Presentation, and Treatment of Pediatric and Adolescent Meniscal Root Injuries, Orthop. J. Sports Med. 6 (2018) 1–7. https://doi.org/10.1177/2325967118803888.
[39] A.C. Abraham, H.M. Pauly, T.L. Haut Donahue, Deleterious effects of osteoarthritis on the structure and function of the meniscal enthesis, Osteoarthritis Cartilage 22 (2014) 275–283. https://doi.org/10.1016/j.joca.2013.11.013.
[40] T.L. Haut Donahue, H.M. Pauly, Osteoarthritic meniscal entheses exhibit altered collagen fiber orientation, Connect. Tissue Res. 0 (2021) 1–5. https://doi.org/10.1080/03008207.2021.1890723.
[41] G.M. Genin, A. Kent, V. Birman, B. Wopenka, J.D. Pasteris, P.J. Marquez, S. Thomopoulos, Functional grading of mineral and collagen in the attachment of tendon to bone, Biophys. J. 97 (2009) 976–985. https://doi.org/10.1016/j.bpj.2009.05.043.
[42] Y.-C. Tien, T.-T. Chih, J.-H.C. Lin, C.-P. Ju, S.-D. Lin, Augmentation of tendon-bone healing by the use of calcium-phosphate cement, J. Bone Joint Surg. Br. 86-B (2004) 1072–1076. https://doi.org/10.1302/0301-620X.86B7.14578.
[43] J.Z. Paxton, K. Donnelly, R.P. Keatch, K. Baar, L.M. Grover, Factors Affecting the Longevity and Strength in an In Vitro Model of the Bone–Ligament Interface, Ann. Biomed. Eng. 38 (2010) 2155–2166. https://doi.org/10.1007/s10439-010-0044-0.
[44] H. Mutsuzaki, M. Sakane, H. Nakajima, A. Ito, S. Hattori, Y. Miyanaga, N. Ochiai, J. Tanaka, Calcium-phosphate-hybridized tendon directly promotes regeneration of tendon-bone insertion, J. Biomed. Mater. Res. A 70A (2004) 319–327. https://doi.org/10.1002/jbm.a.30084.
[45] J. Guo, C. Ning, X. Liu, Bioactive calcium phosphate silicate ceramic surface-modified PLGA for tendon-to-bone healing, Colloids Surf. B Biointerfaces 164 (2018) 388–395. https://doi.org/10.1016/j.colsurfb.2018.02.001.
[46] W. Su, J. Guo, J. Xu, K. Huang, J. Chen, J. Jiang, G. Xie, J. Zhao, S. Zhao, C. Ning, Gradient composite film with calcium phosphate silicate for improved tendon -to-Bone intergration, Chem. Eng. J. 404 (2021) 126473. https://doi.org/10.1016/j.cej.2020.126473.
[47] M. Yu, D. Luo, J. Qiao, J. Guo, D. He, S. Jin, L. Tang, Y. Wang, X. Shi, J. Mao, S. Cui, Y. Fu, Z. Li, D. Liu, T. Zhang, C. Zhang, Z. Li, Y. Zhou, Y. Liu, A hierarchical bilayer architecture for complex tissue regeneration, Bioact. Mater. 10 (2022) 93–106. https://doi.org/10.1016/j.bioactmat.2021.08.024.
[48] X. Huangfu, J. Zhao, Tendon-Bone Healing Enhancement Using Injectable Tricalcium Phosphate in a Dog Anterior Cruciate Ligament Reconstruction Model, Arthrosc. J. Arthrosc. Relat. Surg. 23 (2007) 455–462. https://doi.org/10.1016/j.arthro.2006.12.031.

[49] G.M. Kuang, W.P. Yau, W.W. Lu, K.Y. Chiu, Use of a strontium-enriched calcium phosphate cement in accelerating the healing of soft-tissue tendon graft within the bone tunnel in a rabbit model of anterior cruciate ligament reconstruction, Bone Jt. J. 95-B (2013) 923–928. https://doi.org/10.1302/0301-620X.95B7.30748.
[50] P. He, K.S. Ng, S.L. Toh, J.C.H. Goh, In Vitro Ligament–Bone Interface Regeneration Using a Trilineage Coculture System on a Hybrid Silk Scaffold, Biomacromolecules 13 (2012) 2692–2703. https://doi.org/10.1021/bm300651q.
[51] L.E. Iannucci, A.J. Boys, M.C. McCorry, L.A. Estroff, L.J. Bonassar, Cellular and Chemical Gradients to Engineer the Meniscus-to-Bone Insertion, Adv. Healthc. Mater. 8 (2019) 1800806. https://doi.org/10.1002/adhm.201800806.
[52] X. Liu, J. Wu, K. Qiao, G. Liu, Z. Wang, T. Lu, Z. Suo, J. Hu, Topoarchitected polymer networks expand the space of material properties, Nat. Commun. 13 (2022) 1622. https://doi.org/10.1038/s41467-022-29245-0.
[53] K. Vanaja, R.H. Shobha Rani, Design of Experiments: Concept and Applications of Plackett Burman Design, Clin. Res. Regul. Aff. 24 (2007) 1–23. https://doi.org/10.1080/10601330701220520.
[54] K.-L. TSUI, An Overview of Taguchi Method and Newly Developed Statistical Methods for Robust Design, IIE Trans. 24 (1992) 44–57. https://doi.org/10.1080/07408179208964244.
[55] A fully multiple-criteria implementation of the Sobol′ method for parameter sensitivity analysis - Rosolem - 2012 - Journal of Geophysical Research: Atmospheres - Wiley Online Library, (n.d.). https://agupubs.onlinelibrary.wiley.com/doi/full/10.1029/2011JD016355 (accessed June 4, 2024).
[56] W. Shi, X. Chen, J. Shang, An Efficient Morris Method-Based Framework for Simulation Factor Screening, Inf. J. Comput. 31 (2019) 745–770. https://doi.org/10.1287/ijoc.2018.0836.
[57] J. Mueller, K. Shea, C. Daraio, Mechanical properties of parts fabricated with inkjet 3D printing through efficient experimental design, Mater. Des. 86 (2015) 902–912. https://doi.org/10.1016/j.matdes.2015.07.129.
[58] J. Carpintero, F.A. Canales, J. Fábregas, J. Ávila, Factors and Interactions that Influence the Pressure Drop Across An Air Volume Reducing Device on Low-Pressure Water Distribution Networks, Iran. J. Sci. Technol. Trans. Civ. Eng. 46 (2022) 1433–1443. https://doi.org/10.1007/s40996-021-00682-z.
[59] D. Scott-Drechsel, Z. Su, K. Hunter, M. Li, R. Shandas, W. Tan, A new flow co-culture system for studying mechanobiology effects of pulse flow waves, Cytotechnology 64 (2012) 649–666. https://doi.org/10.1007/s10616-012-9445-2.
[60] M.M. Schuff, J.P. Gore, E.A. Nauman, A mixture theory model of fluid and solute transport in the microvasculature of normal and malignant tissues. II: Factor sensitivity analysis, calibration, and validation, J. Math. Biol. 67 (2013) 1307–1337. https://doi.org/10.1007/s00285-012-0544-7.
[61] H. Yang, K.D. Butz, D. Duffy, G.L. Niebur, E.A. Nauman, R.P. Main, Characterization of cancellous and cortical bone strain in the in vivo mouse tibial loading model using microCT-based finite element analysis, Bone 66 (2014) 131–139. https://doi.org/10.1016/j.bone.2014.05.019.
[62] S. Thomopoulos, J.P. Marquez, B. Weinberger, V. Birman, G.M. Genin, Collagen fiber orientation at the tendon to bone insertion and its influence on stress concentrations, J. Biomech. 39 (2006) 1842–1851. https://doi.org/10.1016/j.jbiomech.2005.05.021.

[63] A. Moustafa, T. Sugiyama, J. Prasad, G. Zaman, T.S. Gross, L.E. Lanyon, J.S. Price, Mechanical loading-related changes in osteocyte sclerostin expression in mice are more closely associated with the subsequent osteogenic response than the peak strains engendered, Osteoporos. Int. 23 (2012) 1225–1234. https://doi.org/10.1007/s00198-011-1656-4.
[64] A.F. Pereira, B. Javaheri, A.A. Pitsillides, S.J. Shefelbine, Predicting cortical bone adaptation to axial loading in the mouse tibia, J. R. Soc. Interface 12 (2015) 20150590. https://doi.org/10.1098/rsif.2015.0590.
[65] E. Pickering, M.J. Silva, P. Delisser, M.D. Brodt, Y. Gu, P. Pivonka, Estimation of load conditions and strain distribution for in vivo murine tibia compression loading using experimentally informed finite element models, J. Biomech. 115 (2021) 110140. https://doi.org/10.1016/j.jbiomech.2020.110140.
[66] A.F.T. Mak, D.T. Huang, J.D. Zhang, P. Tong, Deformation-induced hierarchical flows and drag forces in bone canaliculi and matrix microporosity, J. Biomech. 30 (1997) 11–18. https://doi.org/10.1016/S0021-9290(96)00121-2.
[67] P. Manfredini, G. Cocchetti, G. Maier, A. Redaelli, F.M. Montevecchi, Poroelastic finite element analysis of a bone specimen under cyclic loading, J. Biomech. 32 (1999) 135–144. https://doi.org/10.1016/S0021-9290(98)00162-6.
[68] A.F.T. Mak, J.D. Zhang, Numerical Simulation of Streaming Potentials Due to Deformation-Induced Hierarchical Flows in Cortical Bone, J. Biomech. Eng. 123 (2000) 66–70. https://doi.org/10.1115/1.1336796.
[69] J.H. Hong, M.S. Mun, T.-H. Lim, Strain rate dependent poroelastic behavior of bovine vertebral trabecular bone, KSME Int. J. 15 (2001) 1032–1040. https://doi.org/10.1007/BF03185281.
[70] F.H. Dar, R.M. Aspden, A finite element model of an idealized diarthrodial joint to investigate the effects of variation in the mechanical properties of the tissues, Proc. Inst. Mech. Eng. [H] 217 (2003) 341–348. https://doi.org/10.1243/095441103770802504.
[71] W. Yu, X. Wu, H. Cen, Y. Guo, C. Li, Y. Wang, Y. Qin, W. Chen, Study on the biomechanical responses of the loaded bone in macroscale and mesoscale by multiscale poroelastic FE analysis, Biomed. Eng. OnLine 18 (2019) 122. https://doi.org/10.1186/s12938-019-0741-3.